REPORT DOCUMENTATION PAGE

Form Approved
OMB No. 074-0188

1. AGENCY USE ONLY (Leave blank)	2. REPORT DATE	3. REPORT TYPE AND DATES COVERED
	7/8/02	Final Report 9 Jun 1999 - 30 Jun 2001

4. TITLE AND SUBTITLE
Dynamic Behavior and Shock Absorption Properties of Porous Shape Memory Alloys

5. FUNDING NUMBERS
32525-59300 AE

6. AUTHOR(S)
Dimitris C. Lagoudas

7. PERFORMING ORGANIZATION NAME(S) AND ADDRESS(ES)
Texas Engineering Experiment Station
TAMU Office of Sponsored Research
332 Wisenbaker Engineering Research Center
College Station, TX 77843-3000

8. PERFORMING ORGANIZATION REPORT NUMBER
N00014-99-1-1069

9. SPONSORING / MONITORING AGENCY NAME(S) AND ADDRESS(ES)
Office of Naval Research
Ballston Centre Tower One
800 North Quincy Street
Arlington, VA 222175660

10. SPONSORING / MONITORING AGENCY REPORT NUMBER

11. SUPPLEMENTARY NOTES

12a. DISTRIBUTION / AVAILABILITY STATEMENT
DISTRIBUTION STATEMENT A
Approved for Public Release
Distribution Unlimited

20020715 061

13. ABSTRACT *(Maximum 200 Words)*

Two methods for producing porous NiTi shape memory alloy (SMA) were used in this work: conventional sintering and sintering at elevated pressure using a Hot Isostatic Press. Depending on various parameters such as sintering times and temperatures, as well as initial powder size and compaction, porous specimens have been produced with varying average pore sizes.

The phase transformation temperatures of the porous NiTi specimens were determined using a Differential Scanning Calorimeter, while their microstructure and phase compositions were analyzed using X-Ray Diffraction and a Scanning Electron Microscope aided with Electron-Probe Micro Analysis. Quasi-static and dynamic tests under compression were carried out on various porous NiTi samples to evaluate the pseudo-elasticity and the martensitic detwinning behavior

The effective response of the porous SMAs was modeled using micromechanical averaging techniques. The current work establishes a macroscopic constitutive model for the porous SMA material using the properties of the dense SMA and information about pore shape, volume fraction as well as given pore orientation. A constitutive model for the SMA matrix, which is capable of accounting for the development of plastic strains, was developed as part of the modeling effort. The results from the numerical simulations were compared with the experimental data.

14. SUBJECT TERMS	15. NUMBER OF PAGES
Porous Shape Memory Alloy, Powder Metallurgy, Dynamic Loading, Energy Absorption, Constitutive Modeling, Micromechanics	11
	16. PRICE CODE

17. SECURITY CLASSIFICATION OF REPORT	18. SECURITY CLASSIFICATION OF THIS PAGE	19. SECURITY CLASSIFICATION OF ABSTRACT	20. LIMITATION OF ABSTRACT

Contract Information

Contract Number	N00014-99-1-1069
Title of Research	Dynamic Behavior and Shock Absorption Properties of Porous Shape Memory Alloys
Principal Investigator	Dimitris C. Lagoudas
Organization	Texas A&M University

Technical Section

Technical Objectives

The objectives of the project are:

- To investigate different fabrication techniques for producing porous NiTi shape memory alloy.
- To study the constitutive characteristics of porous SMAs as related to the energy dissipation during the forward and reverse phase transformations under impact loading – shock absorption properties of SMAs.
- To design and perform impact experiments on porous SMA rods, and to correlate theoretical predictions with experimental measurements on energy dissipation.
- To investigate the effect of making SMAs in porous form on enhancing it's damping capacity.
- To develop micromechanical model to characterize the thermomechanical response of porous shape memory alloys.

Technical Approach

Porous NiTi SMA has been fabricated from elemental powders from two different methods: 1) using conventional sintering techniques, 2) sintering at elevated pressure using a Hot Isostatic Press (HIP). Depending on various parameters such as sintering times and temperatures, as well as initial powder size and compaction, porous specimens have been produced with varying average pore sizes, ranging from 20 microns up to ½ mm. Figure 1 shows micrographs of four different pore sizes fabricated from sintering and HIPping.

For the conventional sintering method, high purity powders (> 99%) of Ni (44-90μm) and Ti (< 74μm) / TiH_2 (< 44μm) are proportionately mixed to obtain the starting powder of equi-atomic Ni-Ti composition. The porosity count and pore size is controlled by the size of the initial elemental powders used. A mixture of 5gm of powder are pressed into a green compact pellet at loads ranging from 70MPa to 250MPa. After compaction, the pellet is sintered in an UHP Argon atmosphere at various temperatures ranging from 750°C to 1120°C for times ranging from 9 hours to 48 hours. Porosity levels ranging from 20 to 40% have been achieved.

To fabricate porous NiTi from HIPping, elemental Ni and Ti powders are mixed together with a ratio of 50.6 at.% Ni and loosely packed into a stainless steel canister. The canister is then capped (not air tight seal) placed into the HIP machine, vacuum purged, then backfilled with ultra high purity argon, which is then heated and pressurized to 200MPa via the HIP. During the HIPping process, NiTi is created as a result of diffusion of Ni and Ti species. To promote diffusion, Ni and Ti particle sizes of <20 microns and 99.9% pure are employed. For the large pore specimens, the HIPping cycle is ramped to 950°C at 200MPa for 2.5 hours, long enough to introduce diffusion between the powders. To produce small pore specimens, the HIPping temperature is decreased slightly to 900°C and the time is increased to

6 hours. While in the HIP, the pressure is decreased, allowing the argon pores to expand in the still soft NiTi medium (Figure 10). After HIPping, the canister is annealed in a furnace at 900°C for 6 hours to facilitate further diffusion of the elements and to enhance the porosity of the material. The HIPped material has an open pore structure with an achieved porosity count of 42% and 50% for the large and small pore specimens, respectively.

To verify the shape memory characteristics of the porous NiTi specimens, various material analysis methods have been implemented. Some of these methods include identifying the phase transformation temperatures using a Differential Scanning Calorimeter (DSC) and studying the microstructure and phase compositions using X-Ray Diffraction (XRD) and a Scanning Electron Microscope (SEM) aided with Electron-Probe Micro Analysis (EPMA). The phase analysis, microstructure, pore distribution and phase assemblage are further characterized using optical microscopy and Scanning Electron Microscopy (SEM).

Mechanical tests have also been conducted to study the possibility of using porous NiTi in various structural and energy absorption applications. Quasi-static and dynamic tests under compression were carried out on various samples to evaluate the pseudo-elasticity and the martensitic de-twinning behavior.

The effective response of the porous SMAs is modeled using incremental averaging method. The effect of different pore geometries on the effective behavior is investigated. The current work establishes a macroscopic constitutive model for the porous SMA material using the properties of the dense SMA and information about pore shape, volume fraction as well as given pore orientation. Analytical expressions for the overall elastic and tangent stiffness of the porous SMA material are derived and an evolution equation for the overall transformation strain is also derived. The properties of the porous SMA material are obtained by using the constitutive model for dense SMA to model the matrix and treating the inhomogeneities as elastic phases with stiffness equal to zero.

In order to be able to accurately model the response of porous SMAs under mechanical loading, the constitutive model for the corresponding dense SMA must take into account not only the development of transformation strains, but also the evolution of transformation-induced plastic strains. Thus, a constitutive model, which is capable of accounting for the development of plastic strains was developed as part of the modeling effort.

The micromechanical model treats the porous SMA as a composite material with an SMA matrix and pores as second phase. Only the final expressions of the model are presented here, while the details of the derivation of the model can be found in the cited references. The porous SMA composite is characterized by its effective elastic stiffness $\mathbf{L}$, tangent stiffness $\mathbf{T}$ and effective stress, strain and inelastic strain $\mathbf{\Sigma}$, $\mathbf{E}$ and $\mathbf{E}^{in}$.

The following expressions for the overall elastic stiffness $\mathbf{L}$, tangent stiffness $\mathbf{T}$ and the evolution of the overall inelastic strain $\mathbf{E}^{in}$ have been derived:

$$\mathbf{L} = c^m \mathbf{L}^m \mathbf{A}^{el,m}, \quad \mathbf{T} = c^m \mathbf{T}^m \mathbf{A}^m, \tag{1}$$

$$\dot{\mathbf{E}}^{in} = \underbrace{\left(\mathbf{I} - (\mathbf{A}^{el,m})^{-1}\mathbf{A}^m\right) : \dot{\mathbf{E}}}_{\text{term 1}} + \underbrace{(\mathbf{A}^{el,m})^{-1} : \left\langle \dot{\boldsymbol{\varepsilon}}^{tm} + \dot{\boldsymbol{\varepsilon}}^{pm} + \dot{\mathbf{M}}^m : \boldsymbol{\sigma}^m \right\rangle_m}_{\text{term 2}} - \underbrace{\dot{\mathbf{M}} : \mathbf{\Sigma}}_{\text{term 3}}, \tag{2}$$

where $\mathbf{A}^{el,m}$ is the average *elastic* matrix strain concentration factor, $\mathbf{A}^m$ is the average *instantaneous* matrix strain concentration factors; $\mathbf{L}^m$, $\mathbf{M}^m$, $\mathbf{T}^m$, $\boldsymbol{\varepsilon}^{tm}$ and $\boldsymbol{\varepsilon}^{pm}$ are the matrix elastic stiffness, elastic compliance tangent stiffness, transformation and plastic strain, respectively. c^m is the volume fraction of the matrix phase, which is given in terms of the porosity c^p by $c^m = 1 - c^p$. The average of term $\dot{\boldsymbol{\varepsilon}}^{tm} + \dot{\boldsymbol{\varepsilon}}^{pm} + \dot{\mathbf{M}}^m : \boldsymbol{\sigma}^m$ in the above equation is taken over the matrix phase. Note that the elastic strain

concentration factors mush me calculated assuming elastic behavior of the phases. The above derived equations can easily be generalized for the case of a composite with any number of phases.

The concentration factors $\mathbf{A}^{el,m}$ and $\mathbf{A}^{m}$ are evaluated using the Mori-Tanaka method and the shape of the pores. A detailed analysis has been performed to investigate the effect of different pore shapes on the effective properties of porous SMAs and it has been concluded that a spherical pore shape gives adequate representation of porosity in an SMA with a random distribution of pores. Therefore, a spherical pore shape has been used in the numerical calculations.

Progress

Micrographs of specimens created from conventional sintering and HIPping (large and small pore specimens) are shown in Figure 1.

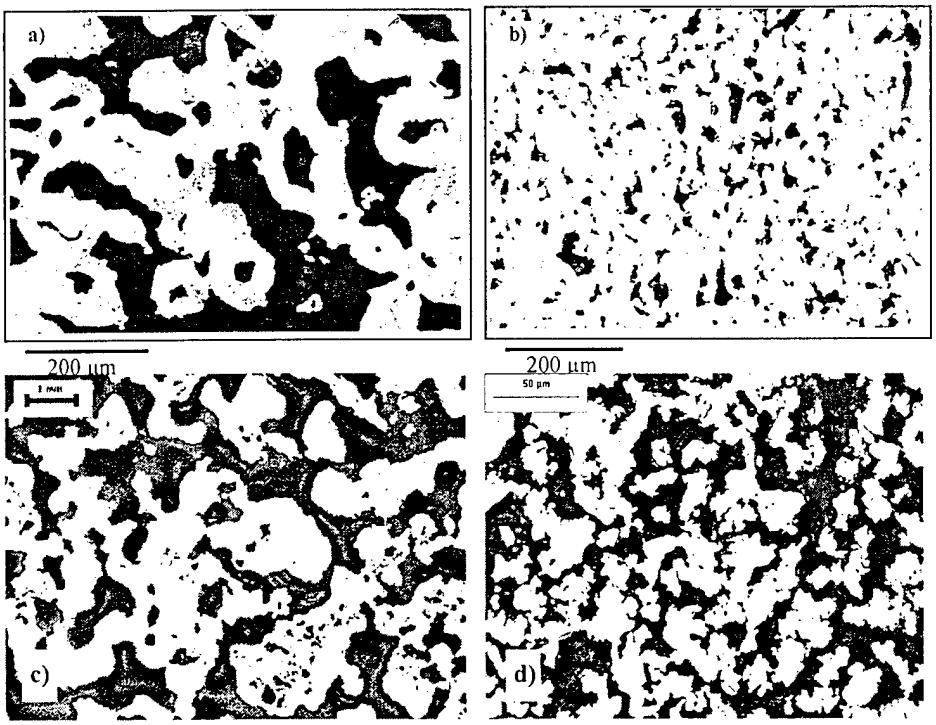

Figure 1. Micrographs of sintered and HIPped porous NiTi: a) sintered with large Ni and Ti powders, b) sintered with small Ni and Ti powders, c) HIPped large pore specimen, d) HIPped small pore specimen.

Electron Microprobe analysis was used to verify the material of the porous specimens created from the sintering and HIPping processes. A preliminary scan for elements was conducted on both types of specimens using an Energy-Dispersive X-ray Spectrometer (EDS). Results for the large and small pore specimens created using the HIP are shown in Figure 2c and 3c, respectively. The EDS shows no evidence of elements other than Ni and Ti, except that of carbon in the small pore specimen from the epoxy casting. Next, by employing the electron backscattering capabilities of the microprobe, evidence of multiple intermetallic phases was revealed (Figures 2a and 3a) in the large and small pore specimens. Evidence of different phases was most prominent in the small pore specimens, with some of the phases confined in areas as large as 20 microns.

Further analysis of the large and small pore specimens using a Wave-Dispersive X-ray Spectrometer (WDS) was conducted on each phase seen in the backscattered electron (BSE) image for quantitative results. For the large pore specimen, the greater part of the material was identified as equiatomic NiTi.

However, the material contains numerous needle-like structures having a width on the order of one-half micron. These needle-like structures were too small to be analyzed without interference from the surrounding medium. By analyzing some of the larger intersections of needle phases however, it is presumed by a slight increase in the percentage of Ni that the needle phases are Ni rich phases. For the small pore specimen, five different phases, i.e., NiTi, Ni_2Ti, $NiTi_3$ and elemental Ni and Ti were identified, as shown in Table I. After identifying the different compounds contained in both types of specimens, the BSE image was further analyzed and area percentages of the phases as well as the pores were calculated. The area percentages of the large pore specimen are shown in Figure 2b and 2d, while the area percentages of the small pore specimen are shown in Figure 3b and 3d. The apparent reason for the presence of relatively large intermetallic phase regions in the small pore specimens is the lower fabrication temperature, which leads to incomplete diffusion of the elemental powders.

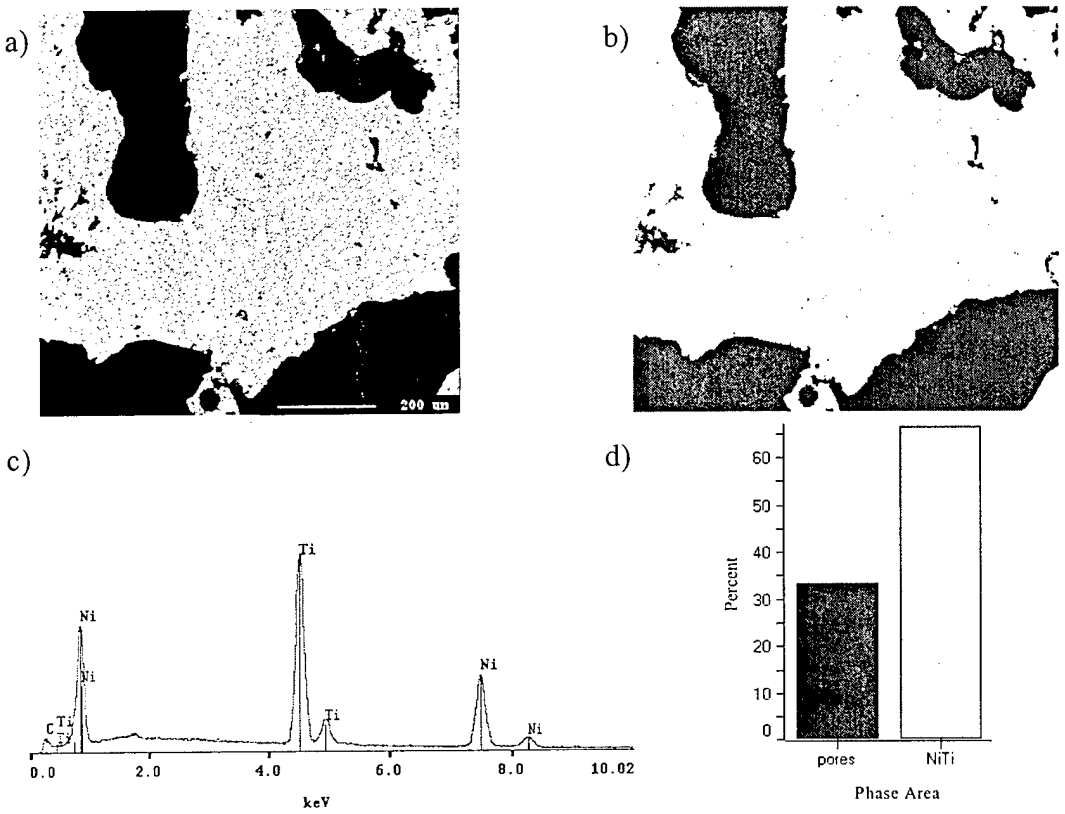

Figure 2: Microprobe analysis of large pore NiTi: (a) BSE image identifying Ni and Ti phases; (b) phase analysis of BSE image after image enhancement; (c) EDS of porous NiTi; (d) percent area of pores and identified phases.

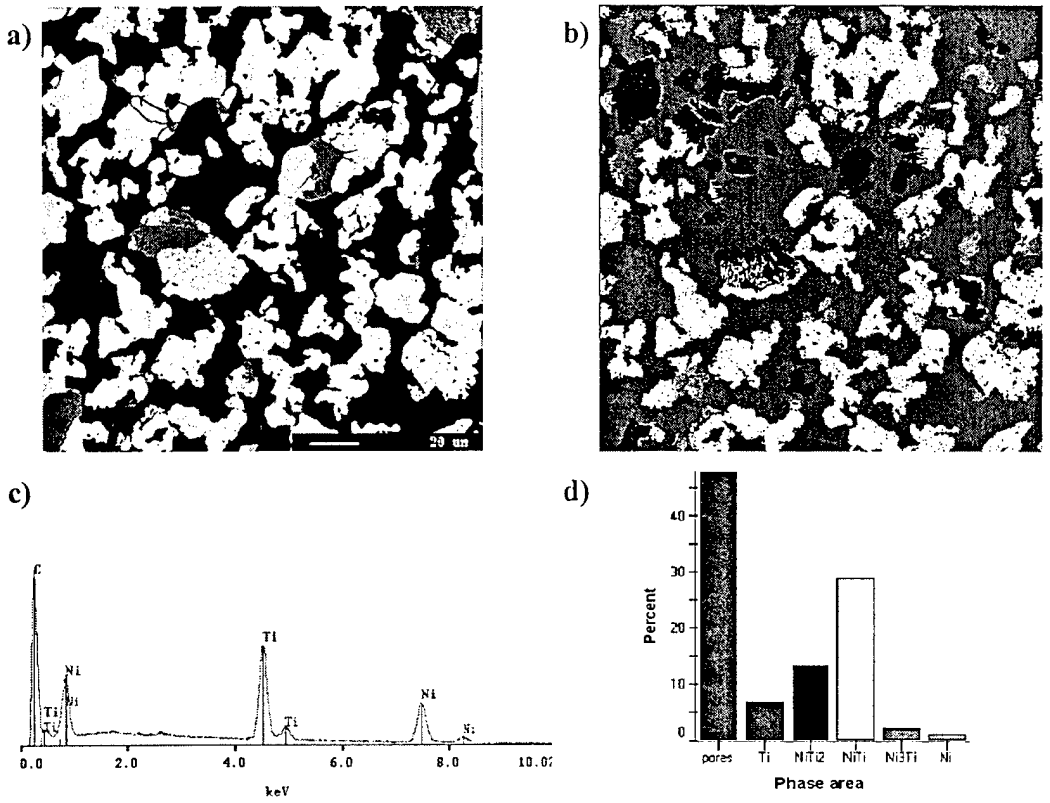

Figure 3: Microprobe analysis of small pore NiTi: (a) BSE image identifying single phases; (b) phase analysis of BSE image after image enhancement; (c) EDS of porous NiTi; (d) percent area of pores and identified phases.

Porous NiTi cylindrical specimens with nominal diameter of 13mm and length of 35mm were mechanically tested under compressive load. Both large and small pore specimens were tested. The porosity of the specimens was measured by taking micrographs of the specimens and estimating the ratio of the area occupied by the pores to the total area at different cross-sections. The estimate of the porosity was also verified by comparing the density of the porous NiTi material with the theoretical density of fully dense NiTi. The porosity of the large pore specimens was estimated to be equal to 42%, while the porosity of the small pore specimens was equal to 50%. The specimens were mechanically tested under compressive load. Load from a hydraulic MTS load frame was applied through two compression plates. An extensometer was used to take the strain measurements during testing. The specimens were tested using a cyclic loading-unloading pattern by loading quasi-statically up to a stress and strain level and then unloading to zero stress. For each subsequent cycle, the stress and/or strain were increased with respect to the previous level. The resulting stress-strain response for typical specimens, tested at a temperature of 60°C is shown in Figure 4 and shows evidence of pseudoelastic behavior upon unloading. However, full strain recovery is not observed, which has been attributed to plastic strain development in the SMA matrix.

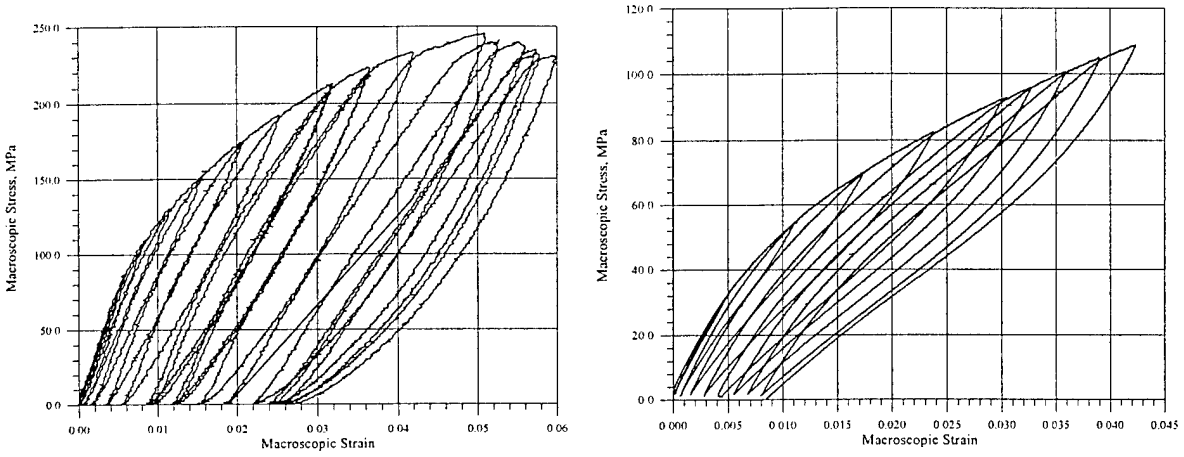

Figure 4. Stress-strain response of porous NiTi SMA bars under compression: (a) large pore specimen; (b) small pore specimen.

Studies in using porous SMAs as energy absorbing joints for impact loads are being conducted. Figure 5 shows four consecutive impact tests performed on the same specimen (reheated to 80°C between each test). The condition of the specimen prior to loading was a mixture of austenite and twinned martensite because the initial testing temperature was slightly below M^{0s}. Therefore, the first part of the stress-strain curves shown in Figure 5 corresponds to elastic loading of austenite and martensite, as well as detwinning of martensite, which progresses to about 0.04 strain. The first phase transformation to stress induced detwinned martensite initiates near a strain of 0.01 (Figure 5, region *A*). After this initial load plateau, a second plateau occurs near a strain of 0.06, indicating further transformation to detwinned martensite and formation of additional inelastic strains which could be attributed to plasticity in the SMA and possible damage (Figure 5, region *B*). Upon unloading, it can be seen that there is partial shape recovery beyond the elastic response of approximately 2%. This could be attributed to the increase in temperature above A^{0s} of the specimen due to latent heat released upon transforming from austenite to martensite and inelastic dissipation. The four consecutive impact tests show good repeatability of the porous NiTi response.

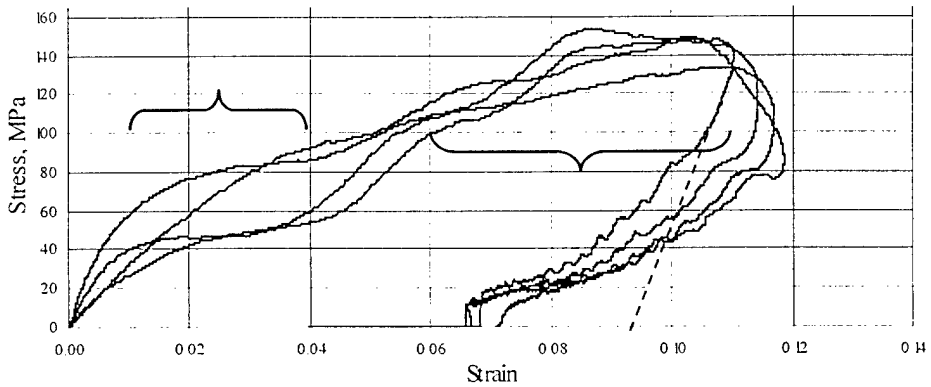

Figure 5. Shape Memory Effect of porous NiTi under impact loading (1 specimen, 4 cycles, 22°C)

Figure 6 shows the results of the first cycle of four impact tests conducted on four different specimens at varying stress and strain levels. The transformation stresses and strains are very similar to the stresses and strains in Figure 5. Again, two distinct plateaus occur at nearly the same stress and strain

levels. The shape recovery beyond the elastic response is measured to be 2%. One noticeable characteristic of the porous NiTi is the ability to undergo considerable inelastic deformation (up to 15% plastic strain) and exhibit nearly the same amount of recoverable strain upon unloading. The repeatability of the transformation curve is consistent, even after the specimen has undergone considerable unrecoverable strain. Again, partial shape recovery is seen upon unloading, contributed to the same reasons as listed for the previous tests seen in Figure 5.

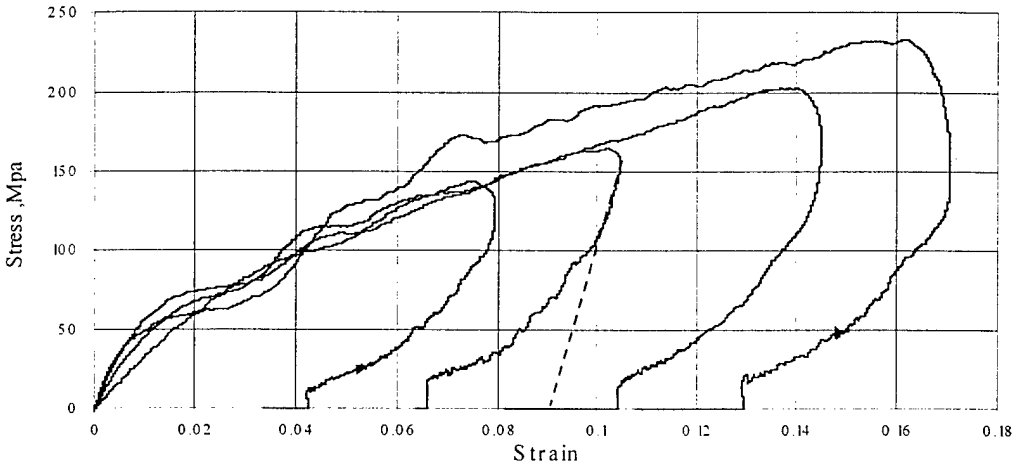

Figure 6. Shape Memory Effect of porous NiTi under impact loading (4 specimens, 22°C)

Figure 7 shows a micrograph of the large pore specimen that was tested in compression under dynamic loading four consecutive cycles (Figure 5). The overall additive strain of the specimen was approximately 16% of the initial length. In contrast, in quasi-static conditions, large pore NiTi specimens generally failed completely near 10% strain. In the loading direction, it can be seen that many of the pores collapsed, causing the specimen to form microcracks throughout the structure while enabling the specimen to withstand near equal amounts of stress for each successive loading cycle.

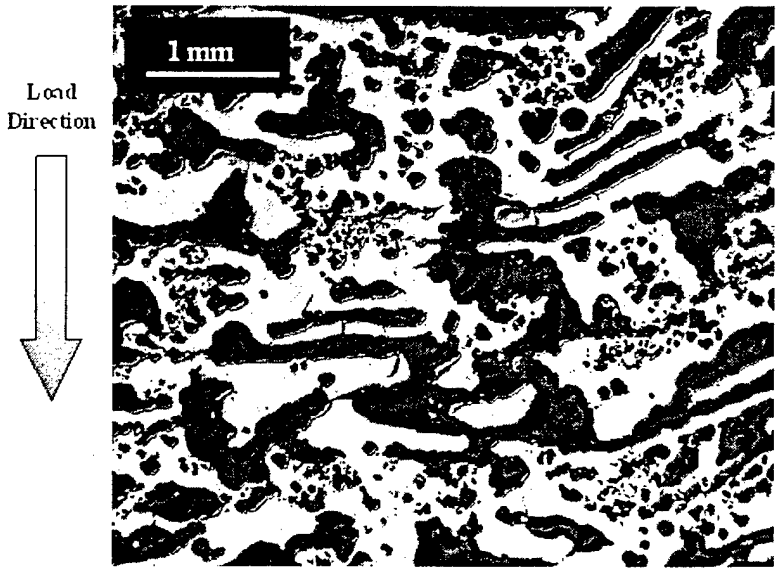

Figure 7. Micrograph of fractured large pore NiTi due to dynamic loading

As a representative example numerical evaluations for the isothermal pseudoelastic response of porous NiTi SMA were performed. The temperature was set to be 70°C. The numerical calculations were performed for an SMA prismatic bar under uniaxial loading. The numerical results were produced using a mesh of two 3-D eight node solid elements, while identical results were obtained for a mesh of eight 3-D elements, since both stress and strain are uniform. The axial effective stress-strain response of the bar for various levels of porosity $c^p = 1 - c^m$ is shown in Figure 8.

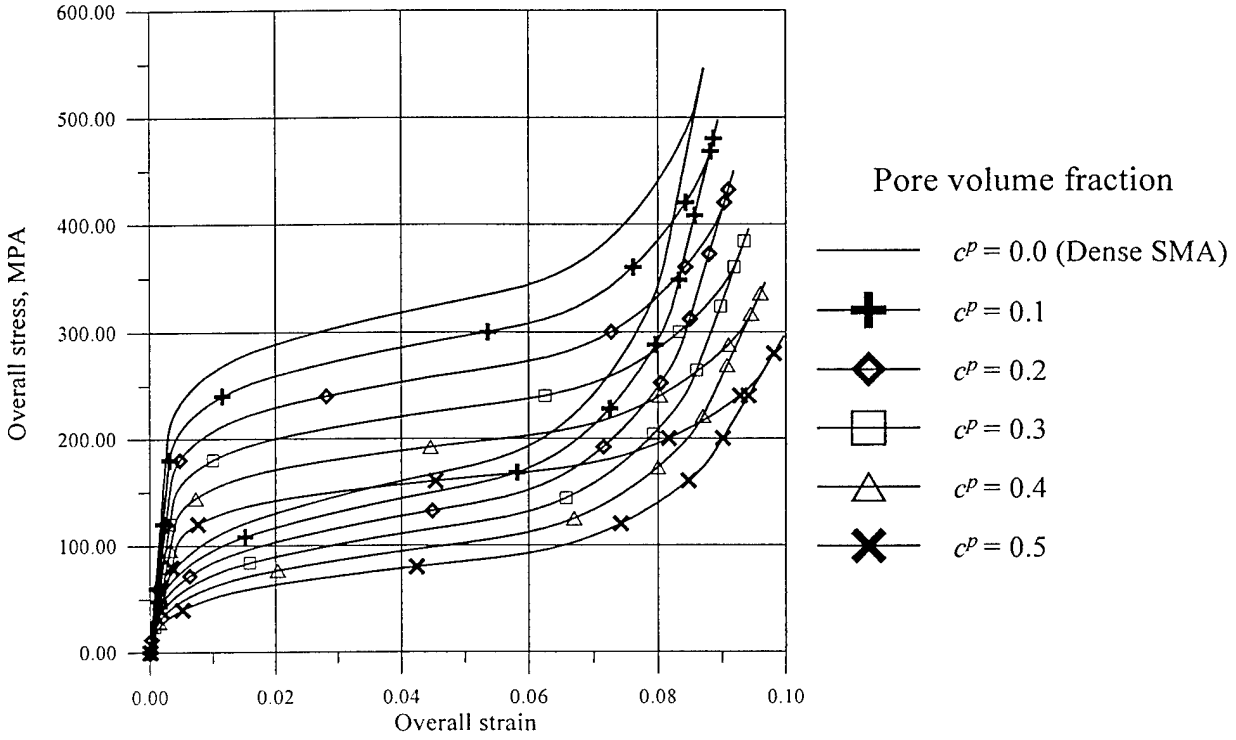

Figure 8. Effective stress-strain response of a porous NiTi SMA bar.

It can be seen from equation (2) that there are three terms contributing to the macroscopic transformation strain. The first term is due to the difference between the elastic and instantaneous strain concentration factors. In the case that $\mathbf{A}^{el,m}$ and $\mathbf{A}^m$ are the same this term will vanish. The second term represents the effect of the inelastic strain rate in the matrix, which has three contributions, one from the transformation strain, the second from the plastic strain and the third from the stiffness change in the matrix. Note that the inelastic strain rate is multiplied by the inverse of the elastic strain concentration factor $(\mathbf{A}^{el,m})^{-1}$. The third term is due to the change in the effective elastic compliance during the phase transformation. The contribution of each of the three terms to the macroscopic inelastic strain $\mathbf{E}^{in}$ is examined for the case of a porous SMA uniaxial bar with NiTi matrix and 50% porosity for the loading path shown in Figure 9a. The normal components in the direction of the loading for each of the three terms contributing to the effective transformation strain are plotted in Figure 9b. It can be seen that the contribution of the second term due to the local transformation and plastic strain is dominant for the current choice of the material parameters.

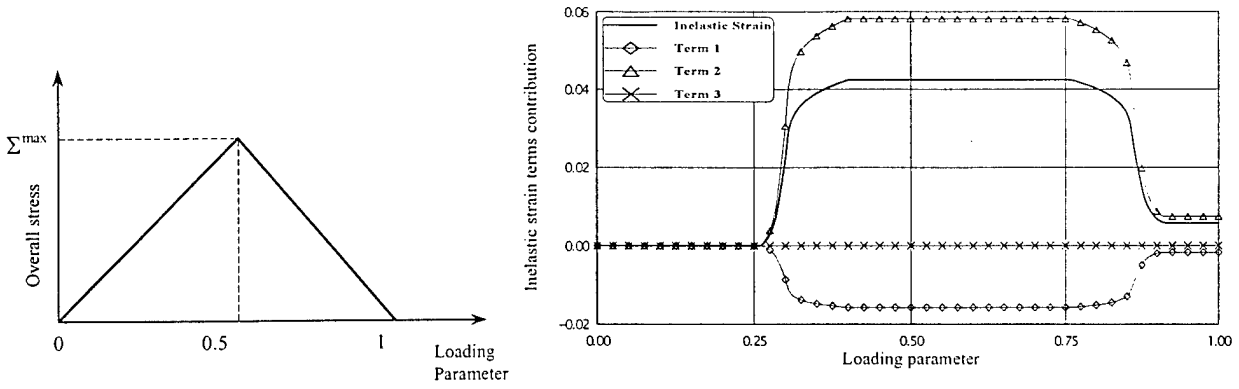

Figure 9. (a) Loading history; (b) Components of the macroscopic inelastic strain as a function of the loading.

The contribution of the first term is negative and lowers the value of the effective macroscopic transformation strain. It can thus be seen from the figure that the effect of the difference between the elastic and instantaneous strain concentration factors is not negligible. The third term, which reflects the effect of the effective elastic compliance change has the smallest magnitude of the three terms. Even though the third term is positive because the elastic compliance of the SMA matrix in the martensitic phase is greater than the compliance in the austenitic phase, its contribution to the total inelastic strain is negative, due to the negative sign in front of the term in equation (2). Note that at the end of the loading/unloading cycle the contribution of the second term does not vanish, since it includes the effect of the plastic strain in the SMA matrix.

To be able to compare the above experimental data with modeling predictions, the corresponding material parameters for the dense SMA matrix need to be evaluated. Assuming that the SMA matrix is isotropic with Poisson's ratio $\nu^A = \nu^M = 0.33$, the Young's elastic moduli of austenite and martensite are evaluated by solving the inverse Mori-Tanaka problem for the porous material and using the experimental data. The value of the effective Young's modulus of the porous austenite is measured using the slope at the beginning of the loading and the corresponding value of the Young's modulus for the austenitic matrix is evaluated from the inverse Mori-Tanaka method. Similarly, the value of the effective Young's modulus of the porous martensite is obtained using the unloading slope. For the case of the large pore porous NiTi the value of the Young's modulus is measured for the last loading cycle before microcracking occurs. The value of the maximum transformation strain is directly measured by extending the unloading slope of the martensite. The transformation temperatures are obtained using the Differential Scanning Calorimeter (DSC) analysis data for the porous SMA. Additional parameters are obtained using the slope of the stress-strain diagram during phase transformation.

The comparison of the compressive stress-strain response for the small pore NiTi alloy simulated by the model with the experimental data is shown in Figure 10a. Overall, very good agreement between the results is obtained. Several observations are made from Figure 10a. First, the effective Young's moduli for both austenite and martensite are correctly reproduced by the model, since their values have been used for the model calibration. The slope of the stress-strain curve during the transformation is in good agreement with the experimental data. The behavior of the material during minor loops is also correctly reproduced. Next, the comparison of the plastic strain predicted by the model with the plastic strain developed during the testing of the material is presented. The evolution of plastic strain in the direction of the loading $\mathbf{E}^p$ is presented as a function of the accumulated detwinned martensitic volume fraction ζ^d. The comparison of the model simulation with the experimental data is shown in Figure 10b. It can be seen that the model simulation closely follows the experimental results.

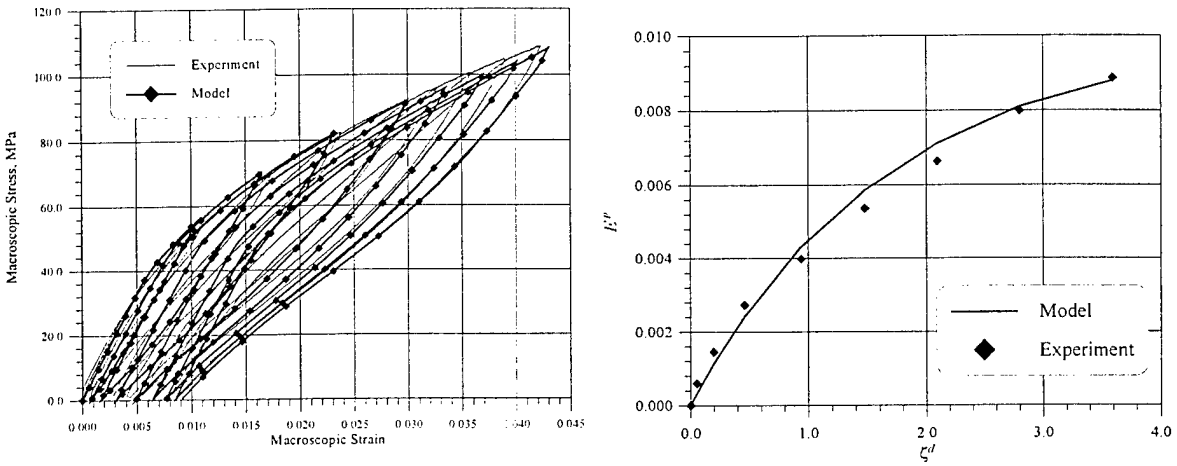

Figure 10. Response of a small pore porous NiTi SMA bar: (a) stress-strain diagram; (b) plastic strain $\mathbf{E}^p$ versus accumulated detwinned martensitic volume fraction ζ^d.

Similar results have been calculated for the large pore porous NiTi alloy. The comparison of the numerical results with the experimental stress-strain data is shown in Figure 11a. It can be seen that the results of the numerical simulations are in good agreement with the experimental data. The plot of the plastic strain versus the accumulated detwinned martensitic volume fraction is shown in Figure 11b.

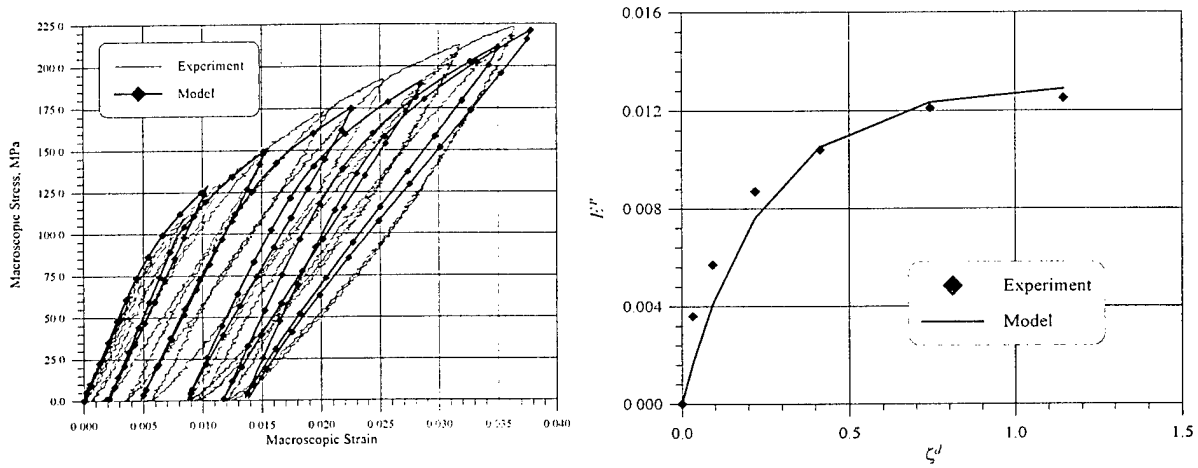

Figure 11. Response of a large pore porous NiTi SMA bar: (a) stress-strain diagram; (b) plastic strain $\mathbf{E}^p$ versus accumulated detwinned martensitic volume fraction ζ^d.

Publications

1. Lagoudas, D. C., Entchev, P. B., Qidwai, M. A., DeGiorgi, V. G., 2000, "Micromechanics of porous shape memory alloys", In: Redmont, J., Main, J. (Eds.), Proceedings of 2000 ASME International Mechanical Engineering Congress & Exposition.
2. Tangaraj, K., Chen, Y.-C., Salama, K., 2000, "Fabrication of porous NiTi shape memory alloy by elemental powder sintering", In: Redmont, J., Main, J. (Eds.), Proceedings of 2000 ASME International Mechanical Engineering Congress & Exposition.
3. Lagoudas, D. C., Entchev, P. B., Vandygriff, E. L., Qidwai, M. A., DeGiorgi, V. G., 2000, "Modeling of thermomechanical response of porous shape memory alloys" In: Lynch, C. S. (Ed.), Proceedings of SPIE, Smart Structures and Materials 2000. Active Materials: Behavior and Mechanics. Vol. 3992.
4. Vandygriff, E. C., Lagoudas, D. C., Thangaraj, K., Chen, Y.-C., 2000, "Porous shape memory alloys Part I: Fabrication and characterization", In: Proceedings of ASC 15th Annual Technical Conference.
5. Qidwai, M. A., Lagoudas, D. C., Entchev, P. B., DeGiorgi, V. G., 2001, "Modeling of the Thermomechanical Behavior of Porous Shape Memory Alloys", International Journal of Solids and Structures, in print.
6. Lagoudas, D. C., Entchev, P. B., 2001, "Modeling Porous Shape Memory Alloys using Micromechanical Averaging Techniques", Mechanics of Materials, accepted for publication.
7. Lagoudas, D. C., Entchev, P. B., 2001, "Micromechanical Modeling of the Behavior of Porous Shape Memory Alloys", In: Proceedings of 6th National Congress on Mechanics, Thessaloniki, Greece.
8. Lagoudas, D. C., Entchev, P. B., Vandygriff, 2001, "Fabrication, Modeling and Characterization of Porous Shape Memory Alloys", In: Proceedings of SPIE 2001 Conference.
9. Lagoudas, D. C., Entchev, P. B., Vandygriff, 2001, "Fabrication and Modeling of Porous Shape Memory Alloys", In: Proceedings of ASC 16th Annual Technical Conference.
10. Lagoudas, D. C., Vandygriff, E. C., Chen, Y.-C., Thangaraj, K., 2001, "Processing and characterization of porous NiTi SMA by conventional and elevated pressure sintering", in preparation.